Atmospheric β-Caryophyllene-Derived Ozonolysis Products at Interfaces

Ariana Gray Bé,[†,I] Hilary M. Chase,[†,◊,I] Yangdongling Liu,[†] Mary Alice Upshur,[†,◊] Yue Zhang,[§,◊] Aashish Tuladhar,[‡] Zizwe A. Chase,[‡] Aleia D. Bellcross,[†] Hong-Fei Wang,[$] Zheming Wang,[‡] Victor S. Batista,[Δ] Scot T. Martin, [§,⊥] Regan J. Thomson,[†,*] and Franz M. Geiger[†,*]

[†]Joint Laboratory for Atmospheric Chemistry, Department of Chemistry, Northwestern University, Evanston, IL 60208, USA; [‡]William R. Wiley Environmental Molecular Sciences Laboratory, Pacific Northwest National Laboratory, Richland, WA 99352, USA; [$]Department of Chemistry and Shanghai Key Laboratory of Molecular Catalysis and Innovative Materials, Fudan University, Shanghai 200438, China; [§]John A. Paulson School of Engineering and Applied Sciences, Harvard University, Cambridge, MA 02138, USA; [⊥]Department of Earth and Planetary Sciences, Harvard University, Cambridge, MA 02138, USA; [Δ]Department of Chemistry, Yale University, 225 Prospect St., New Haven, CT 06520, USA

[I]These authors contributed equally to this work.

***Corresponding authors:** r-thomson@northwestern.edu, geigerf@chem.northwestern.edu

Keywords. Sum frequency generation (SFG) spectroscopy, β-caryophyllene ozonolysis, sesquiterpene chemistry, secondary organic material (SOM), phase-resolved SFG, density functional theory (DFG) calculations

Abstract. By integrating organic synthesis, secondary organic aerosol synthesis and collection, DFT calculations, and vibrational sum frequency generation spectroscopy, we identify close spectral matches between the surface vibrational spectra of β-caryophyllene-derived secondary organic material and those of β-caryophyllene aldehyde and β-caryophyllonic acid at various interfaces. Combined with the record high surface tension depression described previously for

these same oxidation products, we discuss possibilities for an intrinsically chemical origin for cloud activation by terpene-derived surfactants. Although the present study does not unequivocally identify the synthesized and analyzed oxidation products on the β-caryophyllene-derived SOM surfaces, these two compounds appear to be the most surface active out of the series, and have also been foci of previous β-caryophyllene field and laboratory studies. An orientation analysis by phase-resolved SFG spectroscopy reveals a "pincer-like" configuration of the β-caryophyllene oxidation products, albeit on a model quartz surface, that somewhat resembles the orientation of inverse double-tailed surfactants at the surfaces biological systems. The structural information suggests that the less polar moiety of a surface-localized oxidation product, such as those studied here, may be the first site-of-contact for a gas-phase molecule approaching an SOA particle containing surface-active β-caryophyllene oxidation products.

1. Introduction. The atmospheric oxidation of biogenic volatile organic compounds (BVOCs) results in the production of naturally produced secondary organic aerosol (SOA) particles,[1-15] a principal, yet elusive, class of airborne particulate matter that impacts the Earth's radiative budget.[16-19] Given that the particle surface is the first point of contact for surrounding species, interfacial phenomena likely influence key SOA processes.[20-23] Therefore, chemical information regarding the aerosol gas/particle interface is of interest for understanding particle growth,[24-27] heterogeneous chemistry,[28] optical properties,[29-30] and cloud activation.[24, 31-43] Surface-active terpene oxidation products have now been observed at the gas/particle interface for the specific cases of deposited isoprene (C_5)- and α-pinene (C_{10})-derived secondary organic material (SOM).[22, 24, 29, 37, 42, 44]

Here, we report a spectroscopic and structural study on the comparatively more complex species derived from sesquiterpene oxidation,[5] specifically that of β-caryophyllene, the most abundant sesquiterpene BVOC emitted into the atmosphere.[45-51] We are motivated by the fact that reaction products produced from β-caryophyllene ozonolysis have been foci in recent field[52-55] and laboratory[47, 56-58] studies examining atmospheric oxidation of sesquiterpenes. Recently, we synthesized several β-caryophyllene oxidation products for use in Yee *et al.* as tracer standards to identify several of these species in the gas and particle phases within SOM collected in the Central Amazon region using semi-volatile thermal desorption aerosol gas chromatography (SV-TAG).[55] Additionally, we recently reported record cloud activation potentials for these β-caryophyllene oxidation products (Figure 1) from measurements of surface tension that exceed those of SDS[59] more than eight times at equivalent concentrations.[5] In this present work, we take the first steps toward elucidating the interfacial structure and orientation of these molecules benchmarked to the surface of an SOA model synthesized from the ozonolysis of β-caryophyllene.

Probing the interfacial molecular composition of SOM remains challenging, as few techniques are appropriate for nondestructive interfacial analysis while also providing chemical bond specificity. These include mass spectrometry configured to ablate external vs. internal portions of particles[60] and X-ray based methods[60] under ultrahigh vacuum conditions, as well as scanning probes[61] and Raman and infrared spectroscopy under ambient conditions.[62-67] In these cases, the relative signal contribution from the particle surface vs. the particle bulk is small.[68] An additional challenge in the analysis of aerosol particles is that concrete elucidation of proposed oxidation products within SOM mixtures remains indeterminate without the chemical synthesis of molecular standards that otherwise may be difficult to isolate in sufficient amounts or separate

from the complex mixtures in field or laboratory collected material.[15, 21, 23, 31, 52-53, 58, 69-73] While mass spectrometry has long remained the widespread method of choice employed in the aerosol science community,[23, 74-81] surface-selective vibrational spectroscopy[22, 62, 82-85] offers the prospect of complementing such studies by selectively probing SOM interfacial chemistry under ambient conditions, nondestructively, and with capabilities for observing constituents present on the surfaces of SOM as well as obtaining molecular orientation information. Previous work in this area reported on the observation of organic molecules at the interface of aerosol particles deposited on or in contact with solid substrates,[22-23, 25, 44, 82, 86-89] and more recently suspended in air.[29, 90] Now, we combine vibrational sum frequency generation (SFG) spectroscopy, density functional theory (DFT) calculations, and organic synthesis to probe the surface composition of β-caryophyllene-derived SOM and to obtain detailed structural and orientational information of individual molecular constituents on the particle surfaces. By comparing the spectra from the synthesized reference compounds with those observed from the β-caryophyllene-derived SOM in both the C–H and C=O stretching frequency regions, we identify β-caryophyllene aldehyde (**1**), along with β-caryophyllonic acid (**3**), as the most likely surface-localized species. These same species were also found to exhibit the highest and second highest surface activities (and thus estimated cloud activation potentials), respectively, of the oxidation products we previously studied by dynamic surface tension measurements.[5, 21]

2. Experimental and Computational Methods.

2.1. Synthesis of Molecular Standards of Putative β-Caryophyllene-Derived Oxidation Products. The synthesis of all compounds studied here are described in our previous work.[31] In summary, aldehyde and monoacid oxidation products **1**–**4** are prepared from ozonolysis of β-caryophyllene under varied reaction times and ozone generator voltage, followed by either

oxidative or reductive work-up conditions to access the desired product carbonyl functionality. Diacid oxidation products **5** and **6** can be synthesized from β-caryophyllonic acid (**3**) as follows: Iodolactonization of monoacid **3** simultaneously protects the carboxylic acid and alkene moieties, silyl enol ether formation and a subsequent ozonolysis convert the methyl ketone to a carboxylic acid, and iodolactone removal reveals the desired acid product, β-caryophyllinic acid (**5**). β-Nocaryophyllinic acid (**6**) can be accessed through a final ozonolysis of β-caryophyllinic acid (**5**) with oxidative work-up conditions.

2.2 Collection of Synthetic Secondary Organic Material (SOM) Derived from β-Caryophyllene. A comprehensive description of the Harvard flow tube reactor used in this work can be found in our previously published work.[25, 91] Briefly, β-caryophyllene was introduced into the flow tube as a solution of β-caryophyllene (≥98.5%, Sigma-Aldrich Inc.) diluted in 1-butanol (1:625 v/v)[25, 92-93] at selected injection rates that altered the gas-phase concentration in the range of 300–500 ppb, which subsequently changed the organic particle mass loading in the flow tube. 1-Butanol was used as an OH scavenger to ensure that ozonolysis products were generated. Excess ozone (53 ppm) was passed through the reactor with a flow rate of 4 SLPM to ensure β-caryophyllene was fully reacted. Aerosol particle samples were nucleated in the absence of seed particles and collected on Teflon filters (PTFE-47 membrane, pore size 0.45 μm, Z269425, Sigma-Aldrich Inc.) for 7–10 hr, or until saturated, for subsequent SFG analysis. From the flow rate, collection time, collection efficiency, and particle mass concentration (obtained from a scanning mobility particle sizer), the mass of the particles collected on the filters was estimated in the range of 5–14 mg (see Table S6 for more details on SOM collection). All filter samples were sealed using Teflon tape and parafilm, stored in a –20 °C freezer, and warmed to room temperature before breaking the sealant for SFG measurements. No spectral changes were

observed over the course of approximately 1.5 years, suggesting the high stability of the SOM once formed, at least as detected by SFG spectroscopy.

2.3. Vibrational Sum Frequency Generation.

2.3.1. Sample Configurations and SFG Experimental Setup. The synthesized standards, along with β-caryophyllene (≥98.5%, Sigma-Aldrich Inc.), were measured in both the condensed and vapor phases in contact with solid fused silica or calcium fluoride substrates at laboratory ambient temperature and relative humidity in near total internal reflection geometry, though we expect the condensed phase spectra to more accurately reflect the phase states of the compounds present in the collected particle-phase SOM.[23] Vapor phase spectra were taken by exposing an optical window with the equilibrium vapor pressure of the compound being measured, and condensed phase spectra were obtained by measuring a window containing a spin-coated sample. Samples were prepared for measurement by spin-coating the compound, dissolved in a deuterated solvent ($CDCl_3$ and/or CD_3OD), at 3000 rpm onto an optical window. Synthetic SOM was analyzed by pressing an optical window against a Teflon filter containing the collected material. Spectra were measured with *ssp* and *ppp* polarization combinations. The *ssp* polarization combination probes the components of the vibrational transition dipole moments that are oriented perpendicular to the solid substrate,[23] whereas the *ppp* polarization combination needed for detailed orientational analysis[94] probes off-diagonal elements of the second-order susceptibility tensor.

The standard (Northwestern University, 10–15 cm^{-1})[82, 95-96] and high (Pacific Northwestern National Laboratory, 0.6 cm^{-1})[83, 97-99] spectral resolution broadband SFG laser systems used herein for obtaining C–H spectra have been detailed in previous work. For the standard resolution SFG laser system, vapor phase spectra of the synthesized compounds were

taken by adding 1–2 drops of viscous liquid compound to the bottom of a fused silica window, which was then sealed with a Viton O-ring to a home-built Teflon cell and placed on a sample stage. The vapor was allowed to equilibrate for ~10–45 minutes before spectral acquisition. The visible and IR beams were aligned above the sample droplet to probe the vapor/solid (as opposed to liquid/solid) interface. Windows containing spin-coated sample were sealed with a Viton O-ring to the Teflon cell and clamped onto the sample stage prior to measuring condensed phase compound spectra. All optical windows were plasma cleaned for 10–15 minutes prior to sample exposure. The spectra reported here are an average of 4–7 individual spectra each taken for 2 minutes each. Spectra were referenced to the *ppp*-polarized nonresonant SFG response of gold deposited on fused silica to account for the incident IR energy distribution, and frequencies were calibrated using a polystyrene film.[23, 91, 100-101] For the high resolution SFG system, vapor phase compound spectra were acquired by placing 1–2 drops of liquid sample at the edge of a shallow Teflon beaker that was then capped with a fused silica optical window. The vapor was allowed to equilibrate for ~10–45 minutes before spectral data acquisition. For spectra of spin-coated compounds, samples were prepared using the same procedure as stated above. All fused silica windows were placed in an ozone cleaner (Novascan Technologies) for ~10 minutes, and plasma cleaned (PDC-001-HP, Harrick Plasma) for ~15 minutes before depositing sample. The spectra reported are an average of 2–3 individual acquisitions each recorded for 5–10 minutes. The data points in the high-resolution SFG spectra were binned by 5 points, or by 1.73 cm^{-1}, in Igor Pro Version 6.11 (WaveMetrics, Lake Oswego, OR, USA). SFG intensities were normalized to the *ppp*-polarized nonresonant SFG profile of clean z-cut α-quartz, and frequencies were calibrated to a polystyrene film.

SFG spectra collected in the C=O region were measured using a TOPAS (TOPAS-C, Light Conversion) tunable optical parametric amplifier set-up that has been described in detail previously.[102] A schematic of the SFG setup is provided in the Supporting Information (Figure S1). Sample preparation and data collection for obtaining condensed phase C=O spectra were carried out under the same protocol as described above for the standard resolution SFG laser system used for obtaining C–H spectra. All C=O spectra were measured using calcium fluoride optical windows. Spectra were recorded using an automated Python script to measure the IR center wavelengths (5500–6300 nm with 695 nm as the spectrograph center wavelength) that cover the frequency range of interest (~1590–1820 cm^{-1}). Spectra were normalized to the incident IR energy profile by recording a *ppp*-polarized nonresonant spectrum from a gold film deposited on calcium fluoride, and frequencies were calibrated to a polystyrene film measured in the C–H region.[103] We also note that large nonlinear bulk responses from β-nocaryophyllinic acid (**6**) were observed upon slow crystallization of the sample (see Figure S4.1), which is consistent with our earlier reports on molecular chirality in field-collected and synthetic atmospheric aerosol particles.[104-106]

2.3.2. Phase-Resolved Spectra on Quartz. We employ a recently established[83, 107-109] internal heterodyne method to obtain phase-resolved SFG spectra of, and thus structural information on, the β-caryophyllene oxidation products spin-coated on z-cut α-quartz. Phase-resolved SFG responses are obtained directly, and without the need of an additional external local oscillator as seen in conventional heterodyne SFG setups.[110-112] Briefly, when measuring an SFG spectrum of a sample deposited onto z-cut α-quartz, the resulting SFG response contains contributions from (a) the bulk quartz and (b) the molecules adsorbed on the quartz. The nonlinear susceptibility

contribution from the adsorbed layer contains both real and imaginary components. The intensity of the SFG spectrum, *I*, that is directly measured is given by eqn. 1:

$$I \propto \left|\chi^{(2)}_{S,eff}\right|^2 = \left|\chi^{(2)}_{S,Re} + i\chi^{(2)}_{S,Im} + i\chi^{(2)}_{Quartz}\right|^2 \qquad (1).$$

Here, $\chi^{(2)}_{S,eff}$ is the effective nonlinear susceptibility from the surface, $\vec{\chi}^{(2)}_{S,Re}$ is the real part of the nonlinear susceptibility from the adlayer, $\vec{\chi}^{(2)}_{S,Im}$ is the imaginary component of the nonlinear susceptibility, and $\vec{\chi}^{(2)}_{Quartz}$ is the nonlinear response from the quartz bulk. The $\vec{\chi}^{(2)}_{Quartz}$ term is assumed to be off-resonance, therefore remaining a constant throughout the experiment, and $\chi^{(2)}_{S,eff}$ is assumed to contribute much less than $\vec{\chi}^{(2)}_{Quartz}$. Therefore, Eq. 1 can be reduced down to following expressions, Eq. 2 and Eq. 3.

$$I = \left|\vec{\chi}^{(2)}_{\text{Quartz}}\right|^2 + 2\vec{\chi}^{(2)}_{\text{Quartz}} \cdot \vec{\chi}^{(2)}_{\text{S,Im}} + \left|\vec{\chi}^{(2)}_{\text{S}}\right|^2 \qquad (2)$$

$$\approx \left|\vec{\chi}^{(2)}_{\text{Quartz}}\right|^2 + 2\vec{\chi}^{(2)}_{\text{Quartz}} \cdot \vec{\chi}^{(2)}_{\text{S,Im}} \qquad (3)$$

Thus, as long as the azimuthal angle (ϕ) of the quartz substrate is known, the sign of $\vec{\chi}^{(2)}_{S,Im}$ is readily obtained directly.

A brief experimental description for phase-resolved measurements using quartz follows. Synthetic standards **1**–**4** were selected as representatives within our available molecular suite for phase-resolved measurements, and all samples were spin-coated onto z-cut α-quartz (right-handed, size 12.7 x 12.7 x 5 mm, Conex System Technology) analogous to what is described in section 2.3.1. The incident visible and IR beams were focused onto the top side of the quartz piece. Spectra reported herein are an average of 5 individual spectra each acquired for 5 minutes. *ssp*-Polarized spectra of the quartz were obtained at azimuthal angles of ϕ = 0° and ϕ = 180°. The

individual spectra were normalized to the spectrum of clean α-quartz at the same azimuthal angle.

2.4. Computational Methods. Density functional theory (DFT) calculations were employed to aid in spectral interpretation. Similar to our previous work,[113-115] geometries for a number of different conformers of each oxidation product were optimized by using B3LYP[116-118]/6-311G(d,p)[119] via the Gaussian '09 software package located at Yale University.[120] Upon optimization, the harmonic and anharmonic frequencies were calculated in addition to the dipole and polarizability derivatives with respect to each normal mode. We identified Fermi resonances through a previously described procedure[114, 121-122] that employs a multi-mode Fermi resonance Hamiltonian with a frequency cutoff of 10 cm^{-1}. According to this model, if an overtone or combination band is within 10 cm^{-1} of a fundamental vibrational mode, the modes couple and result in a shift in frequencies and intensities dependent on the coupling constant. Additional frequency cutoffs were tested, however, a 10 cm^{-1} cutoff appeared to result in the closest spectral matches across all of the oxidation products.

3. Results and Discussion.

3.1. Comparison of SFG Spectra of β-Caryophyllene-Derived SOM and Oxidation Products: C–H Stretches. First, we compare the polarization-resolved SFG spectra we recorded in the C-H stretching region for the β-caryophyllene oxidation products and the β-caryophyllene-derived SOM surfaces in contact with fused silica (Figure 2). The *ssp*-polarized SFG spectrum of β-caryophyllene-derived SOM contains two distinct peaks around 2943 cm^{-1} and 2860 cm^{-1}. Comparison to the *ssp*-polarized spectra of the oxidation products reveals that all compound spectra also display these two peaks at approximately 2940 ± 5 cm^{-1} and 2860 ± 5 cm^{-1}. An additional peak centered between 2902 and 2912 cm^{-1}, which is not present in the SOM

spectrum, is observed in the spectra of β-caryophyllene, β-nocaryophyllone aldehyde (**2**), β-nocaryophyllonic acid (**4**), and both diacid compounds **5** and **6**. The spectra of β-nocaryophyllone aldehyde (**2**) and β-nocaryophyllinic acid (**6**) also contain a 2963 cm^{-1} peak not observed in the other spectra. In contrast to the other compounds, the *ssp*-polarized SFG spectra of β-caryophyllene aldehyde (**1**) and β-caryophyllonic acid (**3**) contain only two prominent peaks near 2943 cm^{-1} and 2860 cm^{-1}, though β-caryophyllonic acid (**3**) shows a small peak around 2902 cm^{-1}. The *ppp*-polarized SFG spectrum of β-caryophyllene-derived SOM contains one distinct peak centered at 2947 cm^{-1}, while the *ppp*-polarized SFG spectra of compounds **2** and **6** contain an additional prominent peak around 2964 cm^{-1}. The *ppp*-polarized spectra of compounds **1**, **3**, **4**, and **5** as well as β-caryophyllene, however, also contain one identifiable peak, though the spectra of β-caryophyllene and compound **4** contain a possible shoulder near 2920 cm^{-1}. As in the *ppp*-polarized SFG spectrum of β-caryophyllene-derived SOM, one prominent peak centered at 2947 cm^{-1} is observed in the *ppp*-polarized SFG spectra of compounds **1** and **3**.

The *ssp*- and *ppp*-polarized SFG spectra in the C-H stretching region show a best match for β-caryophyllene aldehyde (**1**), as it most closely resembles the *ssp*- and *ppp*-polarized SFG spectra of the β-caryophyllene-derived SOM. β-Caryophyllonic acid (**3**) is an additional close spectral match. As discussed earlier, we recently found that β-caryophyllene aldehyde (**1**) exhibits the highest surface activity in aqueous droplets within the synthesized suite of β-caryophyllene oxidation products, with β-caryophyllonic acid (**3**) as the second most surface active compound in the series.[31] While surface-specific measurements of aqueous media are not directly comparable to those in organic SOM, it may be speculated, based on our SFG results, that compounds **1** and **3** exhibit a higher propensity to populate the surface of SOM than the other compounds studied.

3.2. Comparison of SFG Spectra of β-Caryophyllene-Derived SOM and Oxidation Products: Carbonyl Stretches. Applying our spectral analysis in the C=O stretching region, albeit on calcium fluoride (given its transparency in this infrared region), we find (Figure 3) the following: The SFG spectrum of the β-caryophyllene-derived SOM is remarkably simple, as it contains only one broad peak centered at ~1730 cm^{-1}. Few spectral differences are observed in the oxidation product spectra compared to that of the β-caryophyllene-derived SOM, with the exception of a slight mismatch between the spectral shape and center peak frequency in the SOM and compound **4** spectra in the C=O region. Additionally, the SFG spectrum of diacid compound **6** contains a possible shoulder around 1690 cm^{-1}, which is in contrast to the other spectra. These spectral differences suggest that compounds **4** and **6** may not populate the surface of β-caryophyllene-derived SOM, lending further support to our conclusions from the interfacial tension measurements and the *ssp*- and *ppp*-polarized SFG spectra we collected in the C-H stretching region (*vide supra*).

The SFG spectra of compounds **1**, **2**, **3**, and **5** all contain a broad peak centered near 1730 cm^{-1}, which matches closely to the SFG spectrum of β-caryophyllene-derived SOM. The absence of prominent spectral differences in the C=O region suggests the insensitivity of this region for identifying carbonyl groups on secondary organic material derived from β-caryophyllene with chemical specify. Yet, this same insensitivity offers the opportunity to test generically for the presence of carbonyl groups at the interface by SFG spectroscopy. While the C=O data alone cannot help to distinguish which oxidation products may populate the surface of the SOM, the C–H spectra reveal more notable spectral variances in the oxidation products compared to the SOM.

A thorough analysis of spectral assignments in the C=O region that is based on comparison to carbonyl standards is forthcoming. β-Caryophyllene was also measured as a control and showed no C=O signal by SFG, as expected. We note that the oxidation products gave negligible signal in the *ppp* polarization combination in the C=O region. Taken together, then, the C–H and C=O data together reveal that the spectrum of β-caryophyllene aldehyde (**1**), as well as that of β-caryophyllonic acid (**3**), spectrally resemble the β-caryophyllene-derived SOM surface to a largest degree out of the suite of compounds studied herein.

3.3. Analysis of Phase-Resolved Spectra and Intensity Spectra Using DFT Calculations. Accounting for Fermi resonances as determined by our DFT calculations, we obtain similar mode assignments for the dominant peaks in the experimental SFG spectra of the compounds studied here (Table 1). These assignments resemble those of α-pinene, a molecule that has some similar structural motifs (germinal methyl groups on a four-membered ring) to the compounds studied here.[122-123] Specifically, by SFG and DFT, it was found that a majority of the peak intensity in the SFG spectrum of α-pinene was due to contributions of the methylene group within the four-membered ring, which also exhibited the longest vibrational decoherence lifetimes.[98] There are likely some lower intensity vibrational modes present in the spectrum, but this general assignment holds for the compounds studied here for the dominant peaks.

The phase-resolved SFG spectra are rather similar across oxidation products **1**–**4**, therefore we include a representative *ssp*-polarized phase-resolved SFG spectrum of β-caryophyllene aldehyde (**1**) on α-quartz at an azimuthal angle of 0° in Figure 4A. The interference (difference) SFG spectrum shows a positive peak at 2950–2960 cm^{-1}, a negative peak from 2910–2940 cm^{-1}, and a small negative peak near 2850–2880 cm^{-1}. Based on the vibrational mode assignments and the azimuthal angle of quartz, we identify the sign of $\vec{\chi}^{(2)}_{S,Im}$,

and therefore deduce the orientation of four-membered ring on β-caryophyllene aldehyde (**1**) (and by extension that of the other oxidation products) at the quartz surface (please see Supporting Information section S.5.4). Our analysis indicates that the negative interference peak indicates that the CH_3 groups on the cyclobutane ring face away from the surface, just like its methylene group.

In addition to an "up" versus "down" determination of the discussed stretches on the cyclobutane ring given by the phase-resolved SFG results, a hybrid experimental/DFT method previously published for simulating SFG spectra and carrying out conformational analysis[114, 121] was used to determine the molecular orientation that gives the best matched SFG spectrum (Figure 4B) to the high resolution C–H spectrum of compound 1 spin-coated on fused silica. With this information in mind, the probable orientation of β-caryophyllene aldehyde (1), and by extension, the remaining oxidation products studied, is given in Figure 4C. This orientation is reasonable for a somewhat amphiphilic molecule as it enables hydrogen bonding of the oxygenated groups to the Si–OH groups on the quartz surface. We were unable to obtain phase-resolved spectra within the C=O stretching region; however, the negligible *ppp*-polarized signal intensities suggest that the C=O functional groups within the molecule are aligned nearly perpendicular to the surface, resulting in strong *ssp*-polarized signal intensities. Note that polarization intensity ratio analyses[94] using the *ssp*- and *ppp*-polarized C–H spectra in Figure 2 were unsuccessful due to minimal *ppp* signal for the isolated 2860 cm^{-1} CH_3-symmetric (ring) stretch (see Figure S3.1 in the Supporting Information). Altogether, the orientation analysis of complex molecules on a model surface enabled here by phase-resolved SFG measurements opens the possibility to carry out such analyses on the surfaces of synthetic and field-derived SOM.

Atmospheric Implications and Conclusions. This work integrates organic synthesis, aerosol synthesis and collection, DFT calculations, and SFG spectroscopy to search for the presence of sesquiterpene-derived oxidation products, specifically those derived from β-caryophyllene, on the surfaces of synthetic β-caryophyllene-derived SOM. Polarization-resolved SFG spectra of β-caryophyllene aldehyde (**1**), along with β-caryophyllonic acid (**3**), most closely match those of the β-caryophyllene-derived SOM, both in the C–H and the C=O stretching regions, but especially the former. These two compounds also appear to be the most surface active out of the series based on our previously reported dynamic surface tension measurements, as they lead to the largest depressions of interfacial tension in aqueous droplets.[124] Although the present study cannot unequivocally identify the oxidation products on the β-caryophyllene-derived SOM surface, β-caryophyllene aldehyde (**1**) and β-caryophyllonic acid (**3**) have already been positively identified in several non-surface-specific ambient field SOM[55, 58] and laboratory β-caryophyllene ozonolysis[56-57, 125] studies, though an unambiguous compositional analysis on the SOM examined herein is forthcoming. Nevertheless, our current and recent studies[124] provide concrete lines of evidence supporting that SOM surfaces may be disproportionately populated by a minority subset of compounds that exhibit amphiphilic or surfactant-like properties.

We caution that mismatches between the spectra of the other compounds and that of the SOM may be due to a lack of surface activity of these molecules and therefore a propensity to sit in the bulk of the particles. Although mismatches presumably could be due to surface oscillator orientation changes within the SOM, we do not expect diffusion that may cause molecular orientation changes within the β-caryophyllene-derived particles to be likely at the ambient laboratory relative humidity (RH) conditions (~40% RH) used in this study.[126] Additionally, orientation analysis by phase-resolved SFG spectroscopy reveals a “pincer-like” configuration of

the β-caryophyllene oxidation products, albeit on a model quartz surface, that somewhat resembles the orientation of double-tailed surfactants at the surfaces biological systems. This configuration orients the cyclobutane moiety away from the surface, enabling hydrogen bonding of the terminal oxygenated functional groups to the quartz substrate. Though quartz serves as a distant model system for an actual aerosol particle surface, an analogous orientation at a particle surface may be promoted by the presence of water, inorganic salts, highly oxidized molecules, or any other plausible constituents that could induce polarity, charge density, or hydrogen bonding capabilities at the particle surface. Moreover, the "pincer-like" configuration adopted by the β-caryophyllene oxidation products suggests that the less polar moiety of a surface-localized oxidation product, such as those studied here, may be the first site-of-contact for a gas-phase molecule approaching an aerosol particle. Yet, similar investigations of additional SOM constituents are needed in order to fully realize the implications of understanding interfacial structure and orientation on the heterogeneous chemistry leading to particle growth, cloud activation, and other aerosol processes in the atmosphere.

The observed close spectral matches between β-caryophyllene-derived SOM surfaces and β-caryophyllene aldehyde (**1**) and β-caryophyllonic acid (**3**) presented herein, and the record high surface tension depression described previously[5] for these same oxidation products open the possibility for revealing an intrinsically chemical origin for cloud activation. Indeed, the considerable surface activity points to a high likelihood that these molecules may occupy the surfaces of SOA particles formed from β-caryophyllene oxidation in the atmosphere. Taken together, the discussed interfacial tension and SFG results also suggest that the terpene-derived surfactant pool at SOA particle surfaces may be far less chemically complex than that present in the particle bulk. Such findings on the structure and orientation of terpene-derived oxidation

products and their corresponding SOM at interfaces may improve our understanding of the drivers of heterogeneous processes at SOM surfaces containing such species, and the influence they have on estimated cloud activation potentials.

Supporting Information. Schematic of NU Solstice/TOPAS laser setup; IR and Raman spectra of synthesized oxidation products; supplementary C–H and C=O SFG spectra; Nonlinear bulk responses from β-nocaryophyllinic acid upon crystallization; Supplementary data for phase-resolved SFG experiments; Details of SOM collection.

Corresponding Authors

*E-mail: geigerf@chem.northwestern.edu

*E-mail: r-thomson@northwestern.edu

Present Addresses

◊ Yue Zhang: Aerodyne Research Inc., 45 Manning Road, Billerica, MA 01821

◊ Mary Alice Upshur: Dow Chemical Company, 400 Arcola Rd, Collegeville, PA 19426

◊ Hilary Chase: Allied Inventors, 520 Pike Street, Suite 1520, Seattle, WA 98101

Author Contributions.

I These authors contributed equally to this work.

Notes

The authors declare no competing financial interest.

Acknowledgements. A.G.B., H.M.C., and M.A.U. gratefully acknowledge NSF Graduate Research fellowships. M.A.U. also acknowledges a National Aeronautics and Space Administration Earth and Space (NASA ESS) fellowship and support from a P.E.O. Scholar Award. F.M.G. gratefully acknowledges a Friedrich Wilhelm Bessel Prize from the Alexander von Humboldt Foundation. This work was supported by the National Science Foundation (NSF)

under Grant No. CHE-1607640 and the Environmental Molecular Sciences Laboratory (EMSL)

at Pacific Northwest National Laboratory (PNNL) under user project 49291.

References.

(1) Zhang, X.; McVay, R. C.; Huang, D. D.; Dalleska, N. F.; Aumont, B.; Flagan, R. C.; Seinfeld, J. H. Formation and Evolution of Molecular Products in α-Pinene Secondary Organic Aerosol. *Proceedings of the National Academy of Sciences* **2015**, *112*, 14168-73.

(2) Virtanen, A.; Joutsensaari, J.; Koop, T.; Kannosto, J.; Yli-Pirila, P.; Leskinen, J.; Makela, J. M.; Holopainen, J. K.; Poschl, U.; Kulmala, M.*et al.* An Amorphous Solid State of Biogenic Secondary Organic Aerosol Particles. *Nature* **2010**, *467*, 824-7.

(3) Good, N.; Topping, D. O.; Duplissy, J.; Gysel, M.; Meyer, N. K.; Metzger, A.; Turner, S. F.; Baltensperger, U.; Ristovski, Z.; Weingartner, E.*et al.* Widening the Gap between Measurement and Modelling of Secondary Organic Aerosol Properties? *Atmos. Chem. Phys.* **2010**, *10*, 2577-93.

(4) Wyche, K. P.; Monks, P. S.; Smallbone, K. L.; Hamilton, J. F.; Alfarra, M. R.; Rickard, A. R.; McFiggans, G. B.; Jenkin, M. E.; Bloss, W. J.; Ryan, A. C.*et al.* Mapping Gas-Phase Organic Reactivity and Concomitant Secondary Organic Aerosol Formation: Chemometric Dimension Reduction Techniques for the Deconvolution of Complex Atmospheric Data Sets. *Atmos. Chem. Phys.* **2015**, *15*, 8077-100.

(5) Bé, A. G.; Upshur, M. A.; Liu, P.; Martin, S. T.; Geiger, F. M.; Thomson, R. J. Cloud Activation Potentials for Atmospheric α-Pinene and β-Caryophyllene Ozonolysis Products. *ACS Central Science* **2017**, *3*, 715-25.

(6) Lee, A.; Goldstein, A. H.; Keywood, M. D.; Gao, S.; Varutbangkul, V.; Bahreini, R.; Ng, N. L.; Flagan, R. C.; Seinfeld, J. H. Gas-Phase Products and Secondary Aerosol Yields from the Ozonolysis of Ten Different Terpenes. *Journal of Geophysical Research: Atmospheres* **2006**, *111*,

(7) Iinuma, Y.; Boge, O.; Miao, Y.; Sierau, B.; Gnauk, T.; Herrmann, H. Laboratory Studies on Secondary Organic Aerosol Formation from Terpenes. *Faraday Discussions* **2005**, *130*, 279-94.

(8) Griffin, R. J.; Cocker, D. R.; Flagan, R. C.; Seinfeld, J. H. Organic Aerosol Formation from the Oxidation of Biogenic Hydrocarbons. *Journal of Geophysical Research: Atmospheres* **1999**, *104*, 3555-67.

(9) Atkinson, R.; Arey, J. Atmospheric Chemistry of Biogenic Organic Compounds. *Accounts of Chemical Research* **1998**, *31*, 574-83.

(10) Baltensperger, U.; Kalberer, M.; Dommen, J.; Paulsen, D.; Alfarra, M. R.; Coe, H.; Fisseha, R.; Gascho, A.; Gysel, M.; Nyeki, S.*et al.* Secondary Organic Aerosols from Anthropogenic and Biogenic Precursors. *Faraday Discussions* **2005**, *130*, 265-78.

(11) Kroll, J. H.; Seinfeld, J. H. Chemistry of Secondary Organic Aerosol: Formation and Evolution of Low-Volatility Organics in the Atmosphere. *Atmospheric Environment* **2008**, *42*, 3593-624.

(12) Hallquist, M.; Wenger, J. C.; Baltensperger, U.; Rudich, Y.; Simpson, D.; Claeys, M.; Dommen, J.; Donahue, N. M.; George, C.; Goldstein, A. H.*et al.* The Formation, Properties and Impact of Secondary Organic Aerosol: Current and Emerging Issues. *Atmos. Chem. Phys.* **2009**, *9*, 5155-236.

(13) Goldstein, A. H.; Galbally, I. E. Known and Unexplored Organic Constituents in the Earth's Atmosphere. *Environmental Science & Technology* **2007**, *41*, 1514-21.

(14) Jimenez, J. L.; Canagaratna, M. R.; Donahue, N. M.; Prevot, A. S. H.; Zhang, Q.; Kroll, J. H.; DeCarlo, P. F.; Allan, J. D.; Coe, H.; Ng, N. L.*et al.* Evolution of Organic Aerosols in the Atmosphere. *Science* **2009**, *326*, 1525-9.

(15) Nozière, B.; Kalberer, M.; Claeys, M.; Allan, J.; D'Anna, B.; Decesari, S.; Finessi, E.; Glasius, M.; Grgić, I.; Hamilton, J. F.*et al.* The Molecular Identification of Organic Compounds in the Atmosphere: State of the Art and Challenges. *Chem. Rev.* **2015**, *115*, 3919-83.

(16) John H. Seinfeld, S. N. P. *Atmospheric Chemistry and Physics: From Air Pollution to Climate Change*; 3rd ed.; John Wiley & Sons Hoboken, NJ, 2016.

(17) Council, N. R. *Radiative Forcing of Climate Change: Expanding the Concept and Addressing Uncertainties*; The National Academies Press: Washington, DC, 2005.

(18) Myhre, G., D. Shindell, F.-M. Bréon, W. Collins, J. Fuglestvedt, J. Huang, D. Koch, J.-F. Lamarque, D. Lee, B. Mendoza, T. Nakajima, A. Robock, G. Stephens, T. Takemura and H. Zhang, 2013: Anthropogenic and Natural Radiative Forcing. In: Climate Change 2013: The Physical Science Basis. Contribution of Working Group I to the Fifth Assessment Report of the Intergovernmental Panel on Climate Change [Stocker, T.F., D. Qin, G.-K. Plattner, M. Tignor, S.K. Allen, J. Boschung, A. Nauels, Y. Xia, V. Bex and P.M. Midgley (eds.)]. Cambridge University Press, Cambridge, United Kingdom and New York, NY, USA.

(19) Burrows, J. P.; Tyndall, G. S.; Moortgat, G. K. Photolysis of Chlorine Nitrate at 254 Nm. *J. Phys. Chem.* **1988**, *92*, 4340-8.

(20) Mifflin, A. L.; Velarde, L.; Ho, J.; Psciuk, B. T.; Negre, C. F. A.; Ebben, C. J.; Upshur, M. A.; Lu, Z.; Strick, B. L.; Thomson, R. J.*et al.* Accurate Line Shapes from Sub-1 Cm–1 Resolution Sum Frequency Generation Vibrational Spectroscopy of Α-Pinene at Room Temperature. *The Journal of Physical Chemistry A* **2015**, *119*, 1292-302.

(21) Upshur, M. A.; Strick, B. F.; McNeill, V. F.; Thomson, R. J.; Geiger, F. M. Climate-Relevant Physical Properties of Molecular Constituents for Isoprene-Derived Secondary Organic Aerosol Material. *Atmos. Chem. Phys.* **2014**, *14*, 10731-40.

(22) Ebben, C. J.; Shrestha, M.; Martinez, I. S.; Corrigan, A. L.; Frossard, A. A.; Song, W. W.; Worton, D. R.; Petäjä, T.; Williams, J.; Russell, L. M.*et al.* Organic Constituents on the Surfaces of Aerosol Particles from Southern Finland, Amazonia, and California Studied by Vibrational Sum Frequency Generation. *The Journal of Physical Chemistry A* **2012**, *116*, 8271-90.

(23) Ebben, C. J.; Strick, B. F.; Upshur, M. A.; Chase, H. M.; Achtyl, J. L.; Thomson, R. J.; Geiger, F. M. Towards the Identification of Molecular Constituents Associated with the Surfaces of Isoprene-Derived Secondary Organic Aerosol (Soa) Particles. *Atmos. Chem. Phys.* **2014**, *14*, 2303-14.

(24) McNeill, V. F.; Sareen, N.; Schwier, A. N. In *Atmospheric and Aerosol Chemistry*; McNeill, F. V., Ariya, A. P., Eds.; Springer Berlin Heidelberg: Berlin, Heidelberg, 2014, p 201-59.

(25) Shrestha, M.; Zhang, Y.; Ebben, C. J.; Martin, S. T.; Geiger, F. M. Vibrational Sum Frequency Generation Spectroscopy of Secondary Organic Material Produced by Condensational Growth from Alpha-Pinene Ozonolysis. *The journal of physical chemistry. A* **2013**, *117*, 8427-36.

(26) Tolocka, M. P.; Heaton, K. J.; Dreyfus, M. A.; Wang, S.; Zordan, C. A.; Saul, T. D.; Johnston, M. V. Chemistry of Particle Inception and Growth During Α-Pinene Ozonolysis. *Environmental Science & Technology* **2006**, *40*, 1843-8.

(27) Wang, J.; Wexler, A. S. Adsorption of Organic Molecules May Explain Growth of Newly Nucleated Clusters and New Particle Formation. *Geophysical Research Letters* **2013**, *40*, 2834-8.

(28) George, C.; Ammann, M.; D'Anna, B.; Donaldson, D. J.; Nizkorodov, S. A. Heterogeneous Photochemistry in the Atmosphere. *Chem. Rev.* **2015**, *115*, 4218-58.

(29) Wu, Y.; Li, W.; Xu, B.; Li, X.; Wang, H.; McNeill, V. F.; Rao, Y.; Dai, H.-L. Observation of Organic Molecules at the Aerosol Surface. *The Journal of Physical Chemistry Letters* **2016**, *7*, 2294-7.

(30) Ellison, G. B.; Tuck, A. F.; Vaida, V. Atmospheric Processing of Organic Aerosols. *Journal of Geophysical Research: Atmospheres* **1999**, *104*, 11633-41.

(31) Liu, P.; Song, M.; Zhao, T.; Gunthe, S. S.; Ham, S.; He, Y. C.; Qin, Y. M.; Gong, Z.; Amorim, J. C.; Bertram, A. K.*et al.* Resolving the Mechanism of Hygroscopic Growth and Cloud Condensation Nuclei Activity for Organic Particulate Matter. *Nature Comm.* **2018**, *9*, 4076.

(32) Bé, A. G.; Upshur, M. A.; Liu, P.; Martin, S. T.; Geiger, F. M.; Thomson, R. J. Cloud Activation Potentials for Atmospheric Α-Pinene and Β-Caryophyllene Ozonolysis Products. *ACS Central Science* **2017**

(33) Corrigan, C. E.; Novakov, T. Cloud Condensation Nucleus Activity of Organic Compounds: A Laboratory Study. *Atmospheric Environment* **1999**, *33*, 2661-8.

(34) Cruz, C. N.; Pandis, S. N. The Effect of Organic Coatings on the Cloud Condensation Nuclei Activation of Inorganic Atmospheric Aerosol. *Journal of Geophysical Research: Atmospheres* **1998**, *103*, 13111-23.

(35) Duplissy, J.; Gysel, M.; Alfarra, M. R.; Dommen, J.; Metzger, A.; Prevot, A. S. H.; Weingartner, E.; Laaksonen, A.; Raatikainen, T.; Good, N.*et al.* Cloud Forming Potential of Secondary Organic Aerosol under near Atmospheric Conditions. *Geophysical Research Letters* **2008**, *35*,

(36) Facchini, M. C.; Mircea, M.; Fuzzi, S.; Charlson, R. J. Cloud Albedo Enhancement by Surface-Active Organic Solutes in Growing Droplets. *Nature* **1999**, *401*, 257-9.

(37) Frosch, M.; Bilde, M.; DeCarlo, P. F.; Jurányi, Z.; Tritscher, T.; Dommen, J.; Donahue, N. M.; Gysel, M.; Weingartner, E.; Baltensperger, U. Relating Cloud Condensation Nuclei Activity and Oxidation Level of Α-Pinene Secondary Organic Aerosols. *Journal of Geophysical Research: Atmospheres* **2011**, *116*,

(38) Gill, P. S.; Graedel, T. E.; Weschler, C. J. Organic Films on Atmospheric Aerosol Particles, Fog Droplets, Cloud Droplets, Raindrops, and Snowflakes. *Reviews of Geophysics* **1983**, *21*, 903-20.

(39) Huff Hartz, K. E.; Rosenørn, T.; Ferchak, S. R.; Raymond, T. M.; Bilde, M.; Donahue, N. M.; Pandis, S. N. Cloud Condensation Nuclei Activation of Monoterpene and Sesquiterpene Secondary Organic Aerosol. *Journal of Geophysical Research: Atmospheres* **2005**, *110*,

(40) Nozière, B.; Baduel, C.; Jaffrezo, J.-L. The Dynamic Surface Tension of Atmospheric Aerosol Surfactants Reveals New Aspects of Cloud Activation. *Nature communications* **2014**, *5*, 3335.

(41) Prenni, A. J.; Petters, M. D.; Kreidenweis, S. M.; DeMott, P. J.; Ziemann, P. J. Cloud Droplet Activation of Secondary Organic Aerosol. *J. Geophys. Res. Atmos.* **2007**, *112*,

(42) Prisle, N. L.; Asmi, A.; Topping, D.; Partanen, A. I.; Romakkaniemi, S.; Dal Maso, M.; Kulmala, M.; Laaksonen, A.; Lehtinen, K. E. J.; McFiggans, G.*et al.* Surfactant

Effects in Global Simulations of Cloud Droplet Activation. *Geophysical Research Letters* **2012**, *39*,

(43) Ruehl, C. R.; Davies, J. F.; Wilson, K. R. An Interfacial Mechanism for Cloud Droplet Formation on Organic Aerosols. *Science* **2016**, *351*, 1447-50.

(44) Sareen, N.; Schwier, A. N.; Lathem, T. L.; Nenes, A.; McNeill, V. F. Surfactants from the Gas Phase May Promote Cloud Droplet Formation. *Proceedings of the National Academy of Sciences* **2013**, *110*, 2723-8.

(45) Ault, A. P.; Zhao, D.; Ebben, C. J.; Tauber, M. J.; Geiger, F. M.; Prather, K. A.; Grassian, V. H. Raman Microspectroscopy and Vibrational Sum Frequency Generation Spectroscopy as Probes of the Bulk and Surface Compositions of Size-Resolved Sea Spray Aerosol Particles. *Phys. Chem. Chem. Phys.* **2013**, *15*, 6206-14.

(46) Bonn, B.; Moortgat, G. K. Sesquiterpene Ozonolysis: Origin of Atmospheric New Particle Formation from Biogenic Hydrocarbons. *Geophysical Research Letters* **2003**, *30*,

(47) Fu, P.; Kawamura, K.; Chen, J.; Barrie, L. A. Isoprene, Monoterpene, and Sesquiterpene Oxidation Products in the High Arctic Aerosols During Late Winter to Early Summer. *Environmental Science & Technology* **2009**, *43*, 4022-8.

(48) Hartonen, K.; Parshintsev, J.; Vilja, V.-P.; Tiala, H.; Knuuti, S.; Lai, C. K.; Riekkola, M.-L. Gas Chromatographic Vapor Pressure Determination of Atmospherically Relevant Oxidation Products of Β-Caryophyllene and Α-Pinene. *Atmos. Environ.* **2013**, *81*, 330-8.

(49) Helmig, D.; Ortega, J.; Duhl, T.; Tanner, D.; Guenther, A.; Harley, P.; Wiedinmyer, C.; Milford, J.; Sakulyanontvittaya, T. Sesquiterpene Emissions from Pine Trees − Identifications, Emission Rates and Flux Estimates for the Contiguous United States. *Environmental Science & Technology* **2007**, *41*, 1545-53.

(50) Nguyen, T. L.; Winterhalter, R.; Moortgat, G.; Kanawati, B.; Peeters, J.; Vereecken, L. The Gas-Phase Ozonolysis of [Small Beta]-Caryophyllene (C15h24). Part Ii: A Theoretical Study. *Physical Chemistry Chemical Physics* **2009**, *11*, 4173-83.

(51) Shu, Y.; Atkinson, R. Atmospheric Lifetimes and Fates of a Series of Sesquiterpenes. *Journal of Geophysical Research: Atmospheres* **1995**, *100*, 7275-81.

(52) Winterhalter, R.; Herrmann, F.; Kanawati, B.; Nguyen, T. L.; Peeters, J.; Vereecken, L.; Moortgat, G. K. The Gas-Phase Ozonolysis of [Small Beta]-Caryophyllene (C15h24). Part I: An Experimental Study. *Physical Chemistry Chemical Physics* **2009**, *11*, 4152-72.

(53) Jaoui, M.; Lewandowski, M.; Kleindienst, T. E.; Offenberg, J. H.; Edney, E. O. Β-Caryophyllinic Acid: An Atmospheric Tracer for Β-Caryophyllene Secondary Organic Aerosol. *Geophysical Research Letters* **2007**, *34*,

(54) Parshintsev, J.; Nurmi, J.; Kilpeläinen, I.; Hartonen, K.; Kulmala, M.; Riekkola, M.-L. Preparation of Β-Caryophyllene Oxidation Products and Their Determination in Ambient Aerosol Samples. *Analytical and Bioanalytical Chemistry* **2008**, *390*, 913-9.

(55) Jaoui, M.; Leungsakul, S.; Kamens, R. M. Gas and Particle Products Distribution from the Reaction of Β-Caryophyllene with Ozone. *Journal of Atmospheric Chemistry* **2003**, *45*, 261-87.

(56) Winterhalter, R.; Herrmann, F.; Kanawati, B.; Nguyen, T. L.; Peeters, J.; Vereecken, L.; Moortgat, G. K. The Gas-Phase Ozonolysis of Β-Caryophyllene ($C_{15}h_{24}$). Part I: An Experimental Study. *Physical Chemistry Chemical Physics* **2009**, *11*, 4152-72.

(57) van Eijck, A.; Opatz, T.; Taraborrelli, D.; Sander, R.; Hoffmann, T. New Tracer Compounds for Secondary Organic Aerosol Formation from Β-Caryophyllene Oxidation. *Atmos. Environ.* **2013**, *80*, 122-30.

(58) Yee, L. D.; Isaacman-VanWertz, G.; Wernis, R. A.; Meng, M.; Rivera, V.; Kreisberg, N. M.; Hering, S. V.; Bering, M. S.; Glasius, M.; Upshur, M. A.*et al.* Observations of Sesquiterpenes and Their Oxidation Products in Central Amazonia During the Wet and Dry Seasons. *Atmos. Chem. Phys.* **2018**, *18*, 10433-57.

(59) Kairaliyeva, T.; Aksenenko, E. V.; Mucic, N.; Makievski, A. V.; Fainerman, V. B.; Miller, R. Surface Tension and Adsorption Studies by Drop Profile Analysis Tensiometry. *J. Surf. Deterg.* **2017**1225-41.

(60) Ault, A. P.; Guasco, T. L.; Ryder, O. S.; Baltrusaitis, J.; Cuadra-Rodriguez, L. A.; Collins, D. B.; Ruppel, M. J.; Bertram, T. H.; Prather, K. A.; Grassian, V. H. Inside Versus Outside: Ion Redistribution in Nitric Acid Reacted Sea Spray Aerosol Particles as Determined by Single Particle Analysis. *J. Am. Chem. Soc.* **2013**, *135*, 14528-31.

(61) Hudson, P. K.; Young, M. A.; Kleiber, P. D.; Grassian, V. H. Coupled Infrared Extinction Spectra and Size Distribution Measurements for Several Non-Clay Components of Mineral Dust Aerosol (Quartz, Calcite, and Dolomite). *Atmos. Environ.* **2008**, *42*, 5991-9.

(62) Ault, A. P.; Axson, J. L. Atmospheric Aerosol Chemistry: Spectroscopic and Microscopic Advances. *Anal. Chem.* **2017**, *89*, 430-52.

(63) Bondy, A. L.; Kirpres, R. M.; Merzel, R. L.; Pratt, K. A.; Banasxzak Holl, M. M.; Ault, A. P. Atomic Force Microscopy-Infrared Spectroscopy of Individual Atmospheric Aerosol Particles: Subdiffraction Limit Vibrational Spectroscopy and Morphological Analysis. *Anal. Chem.* **2017**, *89*, 5897-8598.

(64) Ault, A. P.; Zhao, D.; Ebben, C. J.; Tauber, M. J.; Geiger, F. M.; Prather, K. A.; Grassian, V. H. Raman Microspectroscopy and Vibrational Sum Frequency Generation Spectroscopy as Probes of the Bulk and Surface Compositions of Size-Resolved Sea Spray Aerosol Particles. *PCCP* **2013**, *15*, 6206-14.

(65) Corrigan, A. L.; Russell, L. M.; Takahama, S.; Aijala, M.; Ehn, M.; Junninen, H.; Rinne, J.; Petaja, T.; Kulmala, M.; Vogel, A. L.*et al.* Biogenic and Biomass Burning Organic Aerosol in a Boreal Forest at Hyytiala, Finland, During Humppa-Copec 2010. *Atmospheric Chemistry and Physics* **2013**, *13*, 12233-56.

(66) Takahama, S.; Schwartz, R. E.; Russell, L. M.; Macdonald, A. M.; Sharma, S.; Leaitch, W. R. Organic Functional Groups in Aerosol Particles from Burning and Non-Burning Forest Emissions at a High-Elevation Mountain Site. *Atmospheric Chemistry and Physics* **2011**, *11*, 6367-86.

(67) Russell, L. M.; Bahadur, R.; Ziemann, P. J. Identifying Organic Aerosol Sources by Comparing Functional Group Composition in Chamber and Atmospheric Particles. *Proceedings of the National Academy of Sciences of the United States of America* **2011**, *108*, 3516-21.

(68) Ebben, C. J.; Ault, A. P.; Ruppel, M. J.; Ryder, O. S.; Bertram, T. H.; Grassian, V. H.; Prather, K. A.; Geiger, F. M. Size-Resolved Sea Spray Aerosol Particles Studied by Vibrational Sum Frequency Generation. *Journal of Physical Chemistry A* **2013**, *117*, 6589-601.

(69) Heaton, K. J.; Sleighter, R. L.; Hatcher, P. G.; Hall Iv, W. A.; Johnston, M. V. Composition Domains in Monoterpene Secondary Organic Aerosol. *Environmental Science & Technology* **2009**, *43*, 7797-802.

(70) Yasmeen, F.; Vermeylen, R.; Maurin, N.; Perraudin, E.; Doussin, J.-F.; Claeys, M. Characterisation of Tracers for Aging of Α-Pinene Secondary Organic Aerosol Using Liquid Chromatography/Negative Ion Electrospray Ionisation Mass Spectrometry. *Environmental Chemistry* **2012**, *9*, 236-46.

(71) Kahnt, A.; Iinuma, Y.; Blockhuys, F.; Mutzel, A.; Vermeylen, R.; Kleindienst, T. E.; Jaoui, M.; Offenberg, J. H.; Lewandowski, M.; Böge, O.*et al.* 2-Hydroxyterpenylic Acid: An Oxygenated Marker Compound for Α-Pinene Secondary Organic Aerosol in Ambient Fine Aerosol. *Environmental Science & Technology* **2014**, *48*, 4901-8.

(72) Gérard, V.; Nozière, B.; Baduel, C.; Fine, L.; Frossard, A. A.; Cohen, R. C. Anionic, Cationic, and Nonionic Surfactants in Atmospheric Aerosols from the Baltic Coast at Askö, Sweden: Implications for Cloud Droplet Activation. *Environmental Science & Technology* **2016**, *50*, 2974-82.

(73) Zhang, X.; Lambe, A. T.; Upshur, M. A.; Brooks, W. A.; Gray Bé, A.; Thomson, R. J.; Geiger, F. M.; Surratt, J. D.; Zhang, Z.; Gold, A.*et al.* Highly Oxygenated Multifunctional Compounds in Α-Pinene Secondary Organic Aerosol. *Environmental Science & Technology* **2017**, *51*, 5932-40.

(74) Suess, D. T.; Prather, K. A. Mass Spectrometry of Aerosols. *Chemical Reviews* **1999**, *99*, 3007-36.

(75) Laskin, A.; Laskin, J.; Nizkorodov, S. A. Mass Spectrometric Approaches for Chemical Characterisation of Atmospheric Aerosols: Critical Review of the Most Recent Advances. *Environmental Chemistry* **2012**, *9*, 163-89.

(76) Beck, M.; Hoffmann, T. A Detailed Msn Study for the Molecular Identification of a Dimer Formed from Oxidation of Pinene. *Atmos. Environ.* **2016**, *130*, 120-6.

(77) Gross, D. S.; Gälli, M. E.; Kalberer, M.; Prevot, A. S. H.; Dommen, J.; Alfarra, M. R.; Duplissy, J.; Gaeggeler, K.; Gascho, A.; Metzger, A.*et al.* Real-Time Measurement of Oligomeric Species in Secondary Organic Aerosol with the Aerosol Time-of-Flight Mass Spectrometer. *Analytical Chemistry* **2006**, *78*, 2130-7.

(78) Hamilton, J. F.; Lewis, A. C.; Carey, T. J.; Wenger, J. C. Characterization of Polar Compounds and Oligomers in Secondary Organic Aerosol Using Liquid Chromatography Coupled to Mass Spectrometry. *Analytical Chemistry* **2008**, *80*, 474-80.

(79) Ng, N. L.; Canagaratna, M. R.; Zhang, Q.; Jimenez, J. L.; Tian, J.; Ulbrich, I. M.; Kroll, J. H.; Docherty, K. S.; Chhabra, P. S.; Bahreini, R.*et al.* Organic Aerosol Components Observed in Northern Hemispheric Datasets from Aerosol Mass Spectrometry. *Atmos. Chem. Phys.* **2010**, *10*, 4625-41.

(80) Zahardis, J.; Geddes, S.; Petrucci, G. A. Improved Understanding of Atmospheric Organic Aerosols Via Innovations in Soft Ionization Aerosol Mass Spectrometry. *Analytical Chemistry* **2011**, *83*, 2409-15.

(81) Ehn, M.; Thornton, J. A.; Kleist, E.; Sipila, M.; Junninen, H.; Pullinen, I.; Springer, M.; Rubach, F.; Tillmann, R.; Lee, B.*et al.* A Large Source of Low-Volatility Secondary Organic Aerosol. *Nature* **2014**, *506*, 476-9.

(82) Ebben, C. J.; Martinez, I. S.; Shrestha, M.; Buchbinder, A. M.; Corrigan, A. L.; Guenther, A.; Karl, T.; Petäjä, T.; Song, W. W.; Zorn, S. R.*et al.* Contrasting Organic Aerosol Particles from Boreal and Tropical Forests During Humppa-Copec-2010 and Amaze-08 Using Coherent Vibrational Spectroscopy. *Atmos. Chem. Phys.* **2011**, *11*, 10317-29.

(83) Fu, L.; Chen, S.-L.; Wang, H.-F. Validation of Spectra and Phase in Sub-1 Cm-1 Resolution Sum-Frequency Generation Vibrational Spectroscopy through Internal Heterodyne Phase-Resolved Measurement. *J. Phys. Chem. B* **2016**, *120*, 1579-89.

(84) Geiger, F. M. Second Harmonic Generation, Sum Frequency Generation, and Χ (3): Dissecting Environmental Interfaces with a Nonlinear Optical Swiss Army Knife. *Annual Review of Physical Chemistry* **2009**, *60*, 61-83.

(85) K. Kemnitz, K. B., J. M. Hicks, G. R. Pinto, K. B. Eisenthal, T. F. Heinz The Phase of Second-Harmonic Light Generated at an Interface and Its Relation to Absolute Molecular Orientation. *Chemical Physical Letters* **1986**, *131*, 285-90.

(86) Ault, A. P.; Moffet, R. C.; Baltrusaitis, J.; Collins, D. B.; Ruppel, M. J.; Cuadra-Rodriguez, L. A.; Zhao, D.; Guasco, T. L.; Ebben, C. J.; Geiger, F. M.*et al.* Size-Dependent Changes in Sea Spray Aerosol Composition and Properties with Different Seawater Conditions. *Environmental Science & Technology* **2013**, *47*, 5603-12.

(87) Ebben, C. J.; Ault, A. P.; Ruppel, M. J.; Ryder, O. S.; Bertram, T. H.; Grassian, V. H.; Prather, K. A.; Geiger, F. M. Size-Resolved Sea Spray Aerosol Particles Studied by Vibrational Sum Frequency Generation. *The Journal of Physical Chemistry A* **2013**, *117*, 6589-601.

(88) Williams, J.; Crowley, J.; Fischer, H.; Harder, H.; Martinez, M.; Petäjä, T.; Rinne, J.; Bäck, J.; Boy, M.; Dal Maso, M.*et al.* The Summertime Boreal Forest Field Measurement Intensive (Humppa-Copec-2010): An Overview of Meteorological and Chemical Influences. *Atmos. Chem. Phys.* **2011**, *11*, 10599-618.

(89) Kasparian, J.; Wolf, J. P. Ultrafast Laser Spectroscopy and Control of Atmospheric Aerosols. *Physical Chemistry Chemical Physics* **2012**, *14*, 9291-300.

(90) Qian, Y.; Deng, G.-h.; Rao, Y. In Situ Chemical Analysis of the Gas–Aerosol Particle Interface. *Anal. Chem.* **2018**, *90*, 10967-73.

(91) Shrestha, M.; Zhang, Y.; Upshur, M. A.; Liu, P.; Blair, S. L.; Wang, H.-f.; Nizkorodov, S. A.; Thomson, R. J.; Martin, S. T.; Geiger, F. M. On Surface Order and Disorder of Α-Pinene-Derived Secondary Organic Material. *The Journal of Physical Chemistry A* **2015**, *119*, 4609-17.

(92) Gao, Y.; Hall, W. A.; Johnston, M. V. Molecular Composition of Monoterpene Secondary Organic Aerosol at Low Mass Loading. *Environmental Science & Technology* **2010**, *44*, 7897-902.

(93) Zhang, Y.; Sanchez, M. S.; Douet, C.; Wang, Y.; Bateman, A. P.; Gong, Z.; Kuwata, M.; Renbaum-Wolff, L.; Sato, B. B.; Liu, P. F.*et al.* Changing Shapes and Implied Viscosities of Suspended Submicron Particles. *Atmos. Chem. Phys.* **2015**, *15*, 7819-29.

(94) Buchbinder, A. M.; al, e. Method for Evaluating Vibrational Mode Assignments in Surface-Bound Cyclic Hydrocarbons Using Sum-Frequency Generation. *J. Phys. Chem. C* **2011**, *115*, 18284-94.

(95) Buchbinder, A. M.; Ray, N. A.; Lu, J.; Van Duyne, R. P.; Stair, P. C.; Weitz, E.; Geiger, F. M. Displacement of Hexanol by the Hexanoic Acid Overoxidation Product in Alcohol Oxidation on a Model Supported Palladium Nanoparticle Catalyst. *J. Am. Chem. Soc.* **2011**, *133*, 17816-23.

(96) Esenturk, O.; Walker, R. A. Surface Structure at Hexadecane and Halo-Hexadecane Liquid/Vapor Interfaces. *J. Phys. Chem. B* **2004**, *108*, 10631-5.

(97) Velarde, L.; Zhang, X.-y.; Lu, Z.; Joly, A. G.; Wang, Z.; Wang, H.-f. Communication: Spectroscopic Phase and Lineshapes in High-Resolution Broadband Sum

Frequency Vibrational Spectroscopy: Resolving Interfacial Inhomogeneities of "Identical" Molecular Groups. *J. Chem. Phys.* **2011**, *135*,

(98) Mifflin, A. L.; Velarde, L.; Ho, J.; Psciuk, B. T.; Negre, C. F.; Ebben, C. J.; Upshur, M. A.; Lu, Z.; Strick, B. F.; Thomson, R. J.*et al.* Accurate Lineshapes from Sub-1 Cm-1 Resolution Sum Frequency Generation Vibrational Spectroscopy of Å-Pinene at Room Temperature. *J. Phys. Chem. A* **2015**, *119*, 1292-302.

(99) Upshur, M. A.; Chase, H. M.; Strick, B. F.; Ebben, C. J.; Fu, L.; Wang, H.; Thomson, R. J.; Geiger, F. M. Vibrational Mode Assignment of Å-Pinene by Isotope Editing: One Down, Seventy-One to Go. *J. Phys. Chem. A* **2016**, *120*, 2684-90.

(100) Stokes, G. Y.; Buchbinder, A. M.; Gibbs-Davis, J. M.; Scheidt, K. A.; Geiger, F. M. Heterogeneous Ozone Oxidation Reactions of 1-Pentene, Cyclopentene, Cyclohexene, and a Menthenol Derivative Studied by Sum Frequency Generation. *The Journal of Physical Chemistry A* **2008**, *112*, 11688-98.

(101) Buchbinder, A. M.; Weitz, E.; Geiger, F. M. Pentane, Hexane, Cyclopentane, Cyclohexane, 1-Hexene, 1-Pentene, Cis-2-Pentene, Cyclohexene, and Cyclopentene at Vapor/Å-Alumina and Liquid/Å-Alumina Interfaces Studied by Broadband Sum Frequency Generation. *The Journal of Physical Chemistry C* **2010**, *114*, 554-66.

(102) Doğangün, M.; Ohno, P. E.; Liang, D.; McGeachy, A. C.; Bé, A. G.; Dalchand, N.; Li, T.; Cui, Q.; Geiger, F. M. Hydrogen-Bond Networks near Supported Lipid Bilayers from Vibrational Sum Frequency Generation Experiments and Atomistic Simulations. *The Journal of Physical Chemistry B* **2018**, *122*, 4870-9.

(103) Adhikari, N. M.; Premadasa, U. I.; Cimatu, K. L. A. Sum Frequency Generation Vibrational Spectroscopy of Methacrylate-Based Functional Monomers at the Hydrophilic Solid–Liquid Interface. *Physical Chemistry Chemical Physics* **2017**, *19*, 21818-28.

(104) Martinez, I. S.; Peterson, M. D.; Ebben, C. J.; Hayes, P. L.; Artaxo, P.; Martin, S. T.; Geiger, F. M. On Molecular Chirality within Naturally Occurring Secondary Organic Aerosol Particles from the Central Amazon Basin. *PCCP* **2011**, *13*, 12114-22.

(105) Ebben, C. J.; Zorn, S. R.; Lee, S.-B.; Artaxo, P.; Martin, S. T.; Geiger, F. M. Stereochemical Transfer to Atmospheric Aerosol Particles Accompanying the Oxidation of Biogenic Volatile Organic Compound. *GRL* **2011**, *38*, L16807-11.

(106) Ebben, C. J.; Shrestha, M.; Martinez, I. S.; Corrigan, A. L.; Frossard, A. A.; Song, W. W.; Worton, D. R.; Petäjä, T.; Williams, J.; Russell, L. M.*et al.* Organic Constituents on the Surfaces of Aerosol Particles from Southern Finland, Amazonia, and California Studied by Vibrational Sum Frequency Generation. *J. Phys. Chem.* **2012**, *116*, 8271-90.

(107) Wang, H.-F. Sum Frequency Generation Vibrational Spectroscopy (Sfg-Vs) for Complex Molecular Surfaces and Interfaces: Spectral Lineshape Measurement and Analysis Plus Some Controversial Issues. *Prog. Surf. Sci.* **2016**, *91*, 155-82.

(108) Fu, L.; Chen, S.-L.; Gan, W.; Wang, H.-F. Cross-Propagation Sum-Frequency Generation Vibrational Spectroscopy. *Chin. J. Chem. Phys.* **2016**, *29*, 70.

(109) Chen, S.-L.; Fu, L.; Gan, W.; Wang, H.-F. Homogeneous and Inhomogeneous Broadenings and the Voigt Line Shapes in the Phase-Resolved and Intensity Sum-Frequency Generation Vibrational Spectroscopy. *J. Chem. Phys.* **2016**, *144*, 034704.

(110) Mathi, P.; Jagatap, B. N.; Mondal, J. A. Heterodyne-Detected Sum Frequency Generation Study of Adsorption of I– at Model Paint–Water Interface and Its Relevance to Post-Nuclear Accident Scenario. *The Journal of Physical Chemistry C* **2017**, *121*, 7993-8001.

(111) Shen, Y. R. Phase-Sensitive Sum Frequency Spectroscopy. *Annu. Rev. Phys. Chem.* **2013**, *64*, 129-50.

(112) Nihonyanagi, S.; Mondal, J. A.; Yamaguchi, S.; Tahara, T. Structure and Dynamics of Interfacial Water Structure Studied by Heterodyne-Detected Vibrational-Sum Frequency Generation. *Annu. Rev. Phys. Chem.* **2013**, *64*, 579-603.

(113) Chase, H. M.; Chen, S.; Fu, L.; Alice Upshur, M.; Rudshteyn, B.; Thomson, R. J.; Wang, H.-F.; Batista, V. S.; Geiger, F. M. Orientations of Nonlocal Vibrational Modes from Combined Experimental and Theoretical Sum Frequency Spectroscopy. *Chemical Physics Letters*

(114) Chase, H. M.; Rudshteyn, B.; Psciuk, B. T.; Upshur, M. A.; Strick, B. F.; Thomson, R. J.; Batista, V. S.; Geiger, F. M. Assessment of Dft for Computing Sum Frequency Generation Spectra of an Epoxydiol and a Deuterated Isotopologue at Fused Silica/Vapor Interfaces. *J. Phys. Chem. B* **2016**, *120*, 1919-27.

(115) Chase, H. M.; Chen, S.; Fu, L.; Upshur, M. A.; Rudshteyn, B.; Thomson, R. J.; Wang, H.-F.; Batista, V. S.; Geiger, F. M. Orientations of Nonlocal Vibrational Modes from Combined Experimental and Theoretical Sum Frequency Spectroscopy. *Chemical Physics Letters* **2017**, *683*, 199-204.

(116) Becke, A. D. Density□Functional Thermochemistry. Iii. The Role of Exact Exchange. *J. Chem. Phys.* **1993**, *98*, 5648-52.

(117) Lee, C.; Yang, W.; Parr, R. G. Development of the Colle-Salvetti Correlation-Energy Formula into a Functional of the Electron Density. *Phys. Rev. B* **1988**, *37*, 785.

(118) Stephens, P.; Devlin, F.; Chabalowski, C.; Frisch, M. J. *Ab Initio* Calculation of Vibrational Absorption and Circular Dichroism Spectra Using Density Functional Force Fields. *J. Phys. Chem.* **1994**, *98*, 11623-7.

(119) Ditchfield, R.; Hehre, W. J.; Pople, J. A. Self□Consistent Molecular□Orbital Methods. Ix. An Extended Gaussian□Type Basis for Molecular□Orbital Studies of Organic Molecules. *The Journal of Chemical Physics* **1971**, *54*, 724-8.

(120) Frisch, M. J.; Trucks, G. W.; Schlegel, H. B.; Scuseria, G. E.; Robb, M. A.; Cheeseman, J. R.; Scalmani, G.; Barone, V.; Mennucci, B.; Petersson, G. A.*et al.*; rev. C.01 ed.; Gaussian Inc.: Wallingford, CT, 2010.

(121) Chase, H. M.; Chen, S.; Fu, L.; Alice Upshur, M.; Rudshteyn, B.; Thomson, R. J.; Wang, H.-F.; Batista, V. S.; Geiger, F. M. Orientations of Nonlocal Vibrational Modes from Combined Experimental and Theoretical Sum Frequency Spectroscopy. *Chemical Physics Letters* **2017**, *683*, 199-204.

(122) Ho, J.; Psciuk, B. T.; Chase, H. M.; Rudshteyn, B.; Upshur, M. A.; Fu, L.; Thomson, R. J.; Wang, H.-F.; Geiger, F. M.; Batista, V. S. Sum Frequency Generation Spectroscopy and Molecular Dynamics Simulations Reveal a Rotationally Fluid Adsorption State of Α-Pinene on Silica. *J. Phys. Chem. C* **2016**, *120*, 12578-89.

(123) Chase, H. M.; Ho, J.; Upshur, M. A.; Thomson, R. J.; Batista, V. S.; Geiger, F. M. Unanticipated Stickiness of Α-Pinene. *J. Phys. Chem. A* **2017**, *121*, 3239–46.

(124) Be, A.; Upshur, M. A.; Liu, P.; Martin, S. T.; Geiger, F. M.; Thomson, R. J. Cloud Activation Potentials for Atmospheric Α-Pinene and Β-Caryophyllene Ozonolysis Products. *ACS Central Science* **2017**, *3*, 715-25.

(125) Li, Y. J.; Liu, P.; Gong, Z.; Wang, Y.; Bateman, A. P.; Bergoend, C.; Bertram, A. K.; Martin, S. T. Chemical Reactivity and Liquid/Nonliquid States of Secondary Organic Material. *Environmental Science & Technology* **2015**, *49*, 13264-74.

Table 1. General Vibrational Mode Assignment for Oxidation Products of β-Caryophyllene with Largest Signal Intensities as Calculated by Fermi Resonance-Corrected DFT

Scaled Vibrational Frequency [cm^{-1}]	Vibrational Mode
~2940	CH_2-symmetric (ring)
~2860	CH_3-symmetric (ring)

Figure Captions.

Figure 1. β-Caryophyllene-derived oxidation products synthesized and analyzed in this work.

Figure 2. High-resolution *ssp*- and *ppp*-polarized SFG C–H spectra of synthetic β-caryophyllene-derived SOM pressed against fused silica (black trace) compared to β-caryophyllene and synthesized β-caryophyllene oxidation products (**1**–**6**) spin-coated onto fused silica. All maximum SFG intensities have been normalized to 1 and offset for clarity.

Figure 3. Standard resolution *ssp*-polarized SFG C=O spectra of synthetic β-caryophyllene-derived SOM on calcium fluoride (black trace) compared to β-caryophyllene and synthesized β-caryophyllene oxidation products (**1**–**6**) spin-coated onto calcium fluoride. All maximum SFG intensities have been normalized to 1 and offset for clarity.

Figure 4. A) Phase-resolved *ssp*-polarized SFG spectrum of β-caryophyllene aldehyde (**1**) on α-quartz with quartz oriented at $\phi = 0°$; B) Best matched SFG simulation (purple trace) overlaid to experimental high resolution spectrum (black trace) of compound 1 (spin-coated on fused silica); C) Proposed orientation of β-caryophyllene aldehyde (**1**) on the α-quartz surface based on phase-resolved data and comparison of calculated vs. experimental SFG spectra (tilt and twist angles of the assigned Z-axis with respect to surface normal are 70° and 110°, respectively)

Figures.

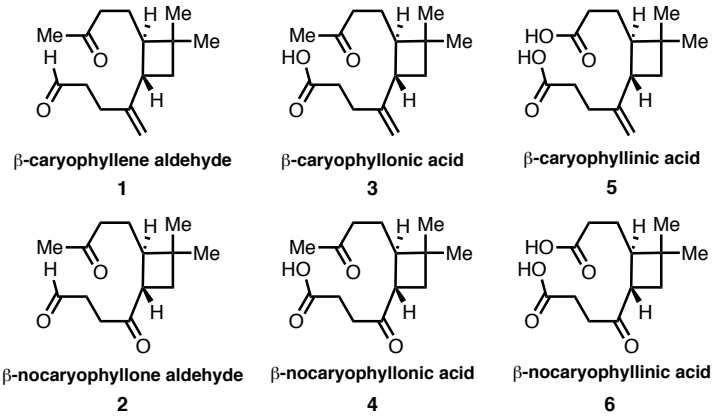

Figure 1.

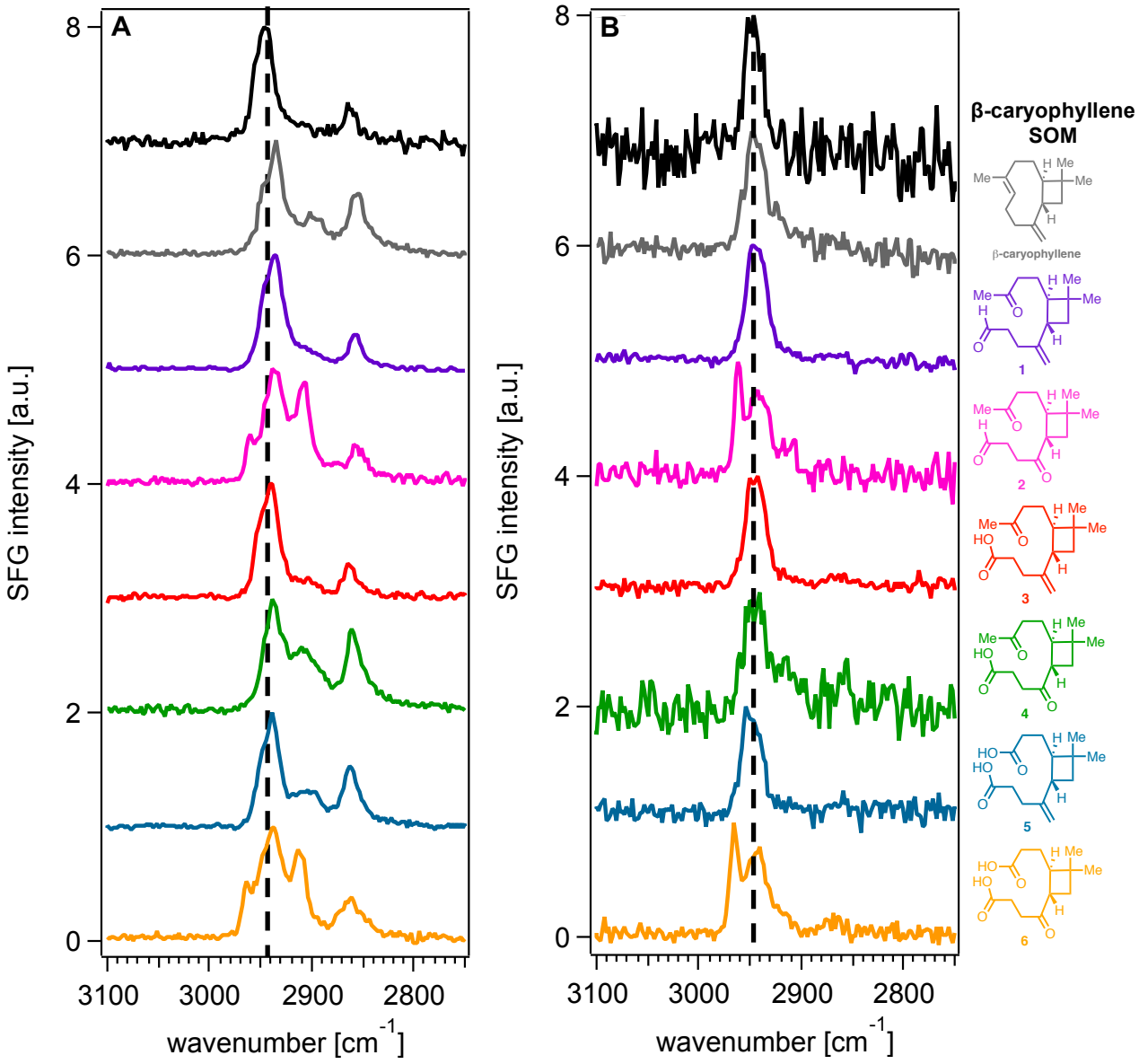
A
B
SFG intensity [a.u.]
wavenumber [cm-1]
3100
3000
2900
2800
0
2
4
6
8
β-caryophyllene
SOM
β-caryophyllene
1
2
3
4
5
6

Figure 2.

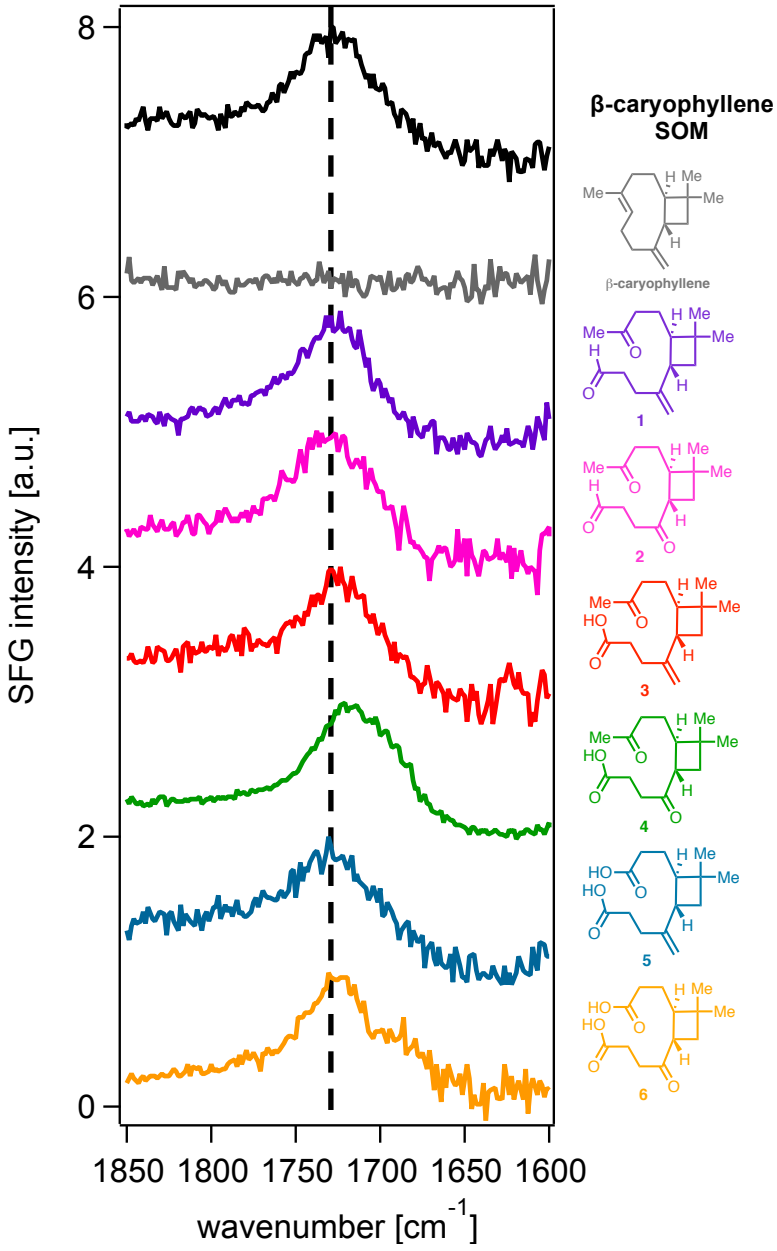
SFG intensity [a.u.]
8
6
4
2
0
1850 1800 1750 1700 1650 1600
wavenumber [cm-1]
β-caryophyllene
SOM
β-caryophyllene
1
2
3
4
5
6

Figure 3.

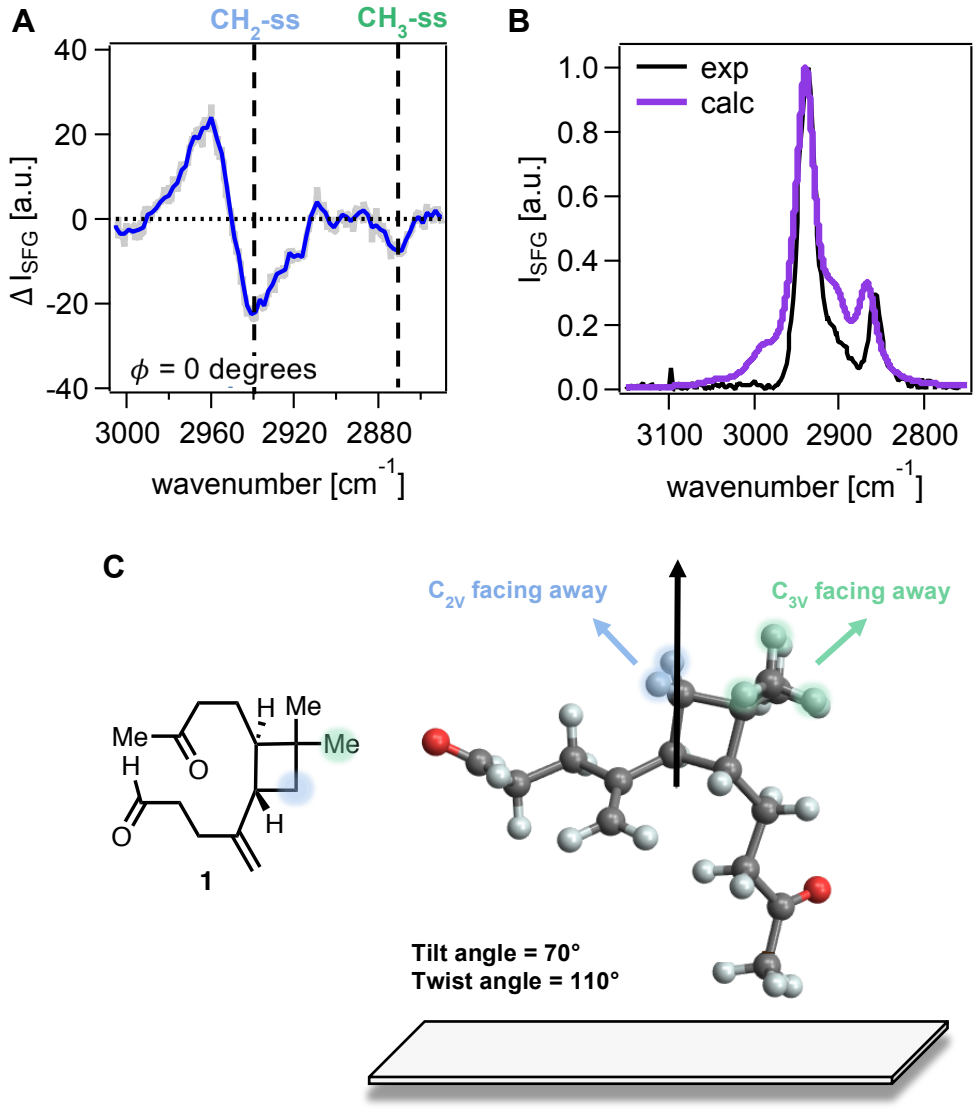
A
CH2-ss
CH3-ss
40
20
0
-20
-40
Δ ISFG [a.u.]
ϕ = 0 degrees
3000 2960 2920 2880
wavenumber [cm-1]
B
1.0
0.8
0.6
0.4
0.2
0.0
ISFG [a.u.]
exp
calc
3100 3000 2900 2800
wavenumber [cm-1]
C
Me
H
O
O
H Me
Me
H
1
C2V facing away
C3V facing away
Tilt angle = 70°
Twist angle = 110°

Figure 4.

TOC Graphic:

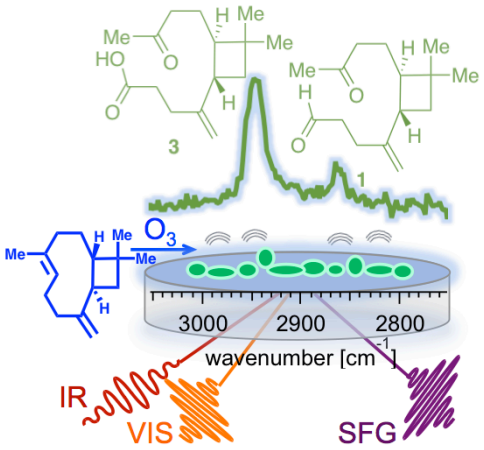
Me
HO
O
H Me
Me
H
3
Me
H
O
H Me
Me
H
1
Me
H Me
Me
H
O3
3000
2900
2800
wavenumber [cm-1]
IR
VIS
SFG